

Available online at *www.ujpronline.com*
Universal Journal of Pharmaceutical Research
An International Peer Reviewed Journal
ISSN: 2831-5235 (Print); 2456-8058 (Electronic)
Copyright©2026; The Author(s): This is an open-access article distributed under the terms of the CC BY-NC 4.0 which permits unrestricted use, distribution, and reproduction in any medium for non-commercial use provided the original author and source are credited

RESEARCH ARTICLE

IN SILICO EVALUATION OF THE INHIBITORY POWER OF AMIDINOUREA DERIVATIVES FOR PHOSPHOPANTETHEINYL TRANSFERASE IN *MYCOBACTERIUM TUBERCULOSIS*

Kouakou Jean-Louis Kouakou[1], Konan Auriol Kra[1], Elvice Akori Esmel[1*], Mélalie Kéïtaépouse Guego[1], Eugene Megnassan[1,2,3]

[1]*Laboratory of Fundamental and Applied Physics, University of Abobo-Adjamé (Now Nangui Abrogoua), Côte d'Ivoire.*
[2]*Laboratory of Constitution and Reaction of Matter, University of Cocody (Now Felix Houphouët Boigny), Côte d'Ivoire.*
[3]*International Centre for Theoretical Physics (ICTP), Strada Costiera, Trieste, Italy.*

Article Info:

Article History:
Received: 22 July 2026
Reviewed: 3 September 2026
Accepted: 8 October 2026
Published: 15 November 2026

Cite this article:
Kouakou KJL, Kra KA, Esmel EA, Kéita M, Megnassan E. *In silico* evaluation of the inhibitory power of amidinourea derivatives for phosphopantetheinyl transferase in *Mycobacterium tuberculosis*. Universal Journal of Pharmaceutical Research 2026; 11(5): 47-61.
http://doi.org/10.22270/ujpr.v11i5.1665

***Address for Correspondence:**
Elvice Akori Esmel, Laboratory of Fundamental and Applied Physics, University of Abobo-Adjamé (Now Nangui Abrogoua), Côte d'Ivoire. Tel: +225-0171020221
E-mail: *esmel.elvice@gmail.com*

Abstract

Background: *Tuberculosis* (*TB*) is an infectious, contagious, and fatal disease, according to the 2025 Global Tuberculosis Report of the World Health Organization (WHO). Phosphopantetheinyl transferase (PptT) is an enzyme that acts as a catalyst in the biosynthesis of cellular lipids in *Mycobacterium tuberculosis*. It is considered potential target for the development of anti-tuberculosis drugs.

Methods: We used molecular docking to establish a quantitative structure-activity relationship (QSAR) model for 25 amidinourea derivatives inhibitors of PptT. The binding free energies, a key physical descriptor, enabled us to elucidate the thermodynamic factors governing the interaction between the enzyme and the inhibitor. This approach, which combines structure-based molecular docking with quantitative modeling, identified specific, critical chemical substituents. This, in turn, led to the development of new derivatives that exhibit potent antitubercular activity.

Results: The resulting QSAR model that accounts for 87% of the variation in biological activity, based on the binding free energies (BFE/PBSA) of the analogues used. Subsequently, an intuitive fragment-replacement approach, based on per-residue interaction energy, which indicates stabilizing interactions, was implemented to identify new analogues. Moreover, 200-ns molecular dynamics simulations have evaluated with satisfaction, the temporal evolution of various properties of the bound inhibitors, such as root mean square deviation (RMSD) from the initial conformation, radius of gyration (rGyr), number of intramolecular hydrogen bonds (intraHB), molecular surface area (molSA), solvent-accessible surface area (SASA), and polar surface area (PSA). The BFE/GBSA of the three best analogs, calculated over the last 50 nanoseconds of the trajectory, align with BFE/PBSA values. Finally, favorable values for the pharmacokinetic descriptors of the best analogues are obtained using the QikProp, pkCSM, and mycoCSM programs.

Conclusion: This study enabled us to identify a new amidinourea analogue AU_1-3-7-9, $IC_{50}^{pre} = 20\ nM$ which is 10 times more active.

Keywords: *Mycobacterium tuberculosis*, Phosphopantetheinyl transferase, molecular docking, amidinourea, molecular dynamics, QSAR.

INTRODUCTION

Tuberculosis (TB) is a chronic and contagious infectious disease caused by the *Mycobacterium tuberculosis* complex (Koch's bacillus)[1]. It generally affects the lungs; hence, the clinical form known as active pulmonary tuberculosis (APT), but it can also affect other parts of the body, in which case it is referred to as extra-pulmonary tuberculosis[2]. TB remains a persistent global health challenge. According to the 2025 Global Tuberculosis Report, the World Health Organization (WHO) estimated approximately 10.7 million cases and 1.23 million deaths in 2024[3]. While significant progress has been made in diagnostic techniques and healthcare accessibility, the emergence of multidrug-resistant tuberculosis (MDR-TB) continues to threaten international recovery efforts. In 2024 alone, an estimated 410,000 individuals

contracted MDR-TB, highlighting a critical need for the discovery of novel therapeutic agents with distinct mechanisms of action[3,4]. To address this threat, recent research has pivoted toward newly validated biological targets. One such promising target is the protein phosphopantetheinyl transferase (PptT), which plays an essential role in the biosynthesis of virulence-critical lipids required for the survival of *Mycobacterium tuberculosis*[5]. Inhibiting PptT offers a strategic pathway to disrupt the pathogen's metabolic integrity. In this study, we explore the *in silico* inhibition of PptT using a series of amidinourea derivatives. Our objective is to establish a univariate QSAR model that correlates the binding free energies (BFE), derived from molecular docking simulations, with the observed experimental activities (the biological response). By utilizing BFE as a primary physical descriptor, we aim to elucidate the thermodynamic factors driving the formation of the enzyme-inhibitor complex. Furthermore, this dual approach, integrating structure-based docking with quantitative modeling, allows us to pinpoint specific chemical substituent at key molecular positions, providing a predictive framework for designing novel derivatives with enhanced anti-tuberculosis potency.

METHODS

Dataset selection and preparation

The chemical dataset for this study consisted of 25 amidinourea derivatives with known experimental biological activities pIC_{50}^{exp} against PptT of *M. tuberculosis*, as reported by Ottavi *et al*.[5]. The spatial geometry of the structures of these ligands was modeled and energy-minimized within the Discovery Studio® (BIOVIA) environment[6]. For the biological target, the crystal structure of phosphopantetheinyl transferase (PptT) in complex with the native ligand Au8918 which occupies the active site as previously described[23,24], was retrieved from the Protein Data Bank (PDB ID: 6CT5)[7]. The protein was prepared using the "Prepare Protein" protocol of Discovery Studio®, which involved adding missing hydrogen atoms, assigning proper ionization states to amino acid residues at pH 7.0, and removing crystallographic water molecules.

Molecular Docking using CDOCKER

Molecular docking simulations were performed using the CDOCKER algorithm, a grid-based method grounded in the CHARMm force field[6]. Water molecules are removed because the docking takes place within the gas. The docking sphere (radius = 10 Å) was centered on the coordinates of the co-crystallized inhibitor within the PptT binding pocket. For each ligand, a series of random conformations were generated and refined through grid-based simulated annealing followed by a final energy minimization. The top-ranked pose for each derivative, characterized by the lowest CDOCKER energy, was selected for subsequent thermodynamic analysis.

Poses selection

For each of the 25 amidinourea derivatives, the CDOCKER algorithm generated a pool of 10 initial docking poses through high-temperature molecular dynamics and subsequent simulated annealing. To select the most energetically relevant orientation for each ligand, poses were initially ranked based on their CDOCKER Energy, which represents the sum of the internal ligand strain and the protein-ligand interaction energy. Following this energy scoring, the top-ranked poses were visually inspected for interaction consistency to ensure their scaffold aligned closely with that of the co-crystallized ligand and that they maintained key interactions observed in the crystal structure, particularly the hydrogen bonding network with the catalytic residue Glu157.

Each protein-ligand complex containing the single best-scoring pose for each ligand that satisfied these structural constraints was then subjected to the "Calculate binding energy" protocol for final binding free energy (ΔG_{bind}) calculation including the loss of conformational entropy of the bound ligand at 298.15K.

Binding Free Energy Calculations with PBSA

To achieve a more accurate physical representation of the binding process, the binding free energies ΔG_{bind} (Eq. 1) calculated for the best poses obtained from docking, using the "Calculate binding energy" protocol; optimal coverage of the conformational space was ensured, and the Poisson-Boltzmann/surface area (PBSA) method an implicit solvation model was applied. The total binding free energy was determined according to the following equation:

$$\Delta G_{bind} = \Delta E_{bind} + \Delta G_{solv} - T\Delta S_{conf} \quad \text{Eq. 1}$$

$$\Delta E_{bind} = E_{complex} - E_{receptor} - E_{ligand} \quad \text{Eq. 2}$$

Where:

- ΔE_{bind} (Eq. 2) represents the gas-phase interaction energy (electrostatic and van der Waals).
- ΔG_{solv} accounts for the solvation free energy, calculated by solving the Poisson-Boltzmann equation. We employed a solvent dielectric constant of 80 and a solute dielectric constant of 4 to represent the protein-ligand environment accurately.
- $-T\Delta S_{conf}$ is the difference between entropic energies of the complex, receptor and ligand. It represents the configurational entropy estimation, accounting for the loss of freedom upon binding.

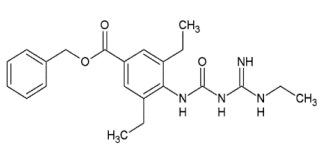
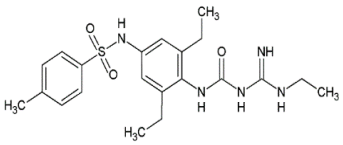
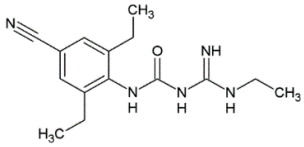
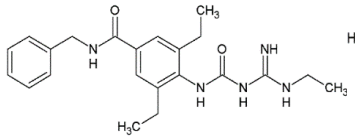
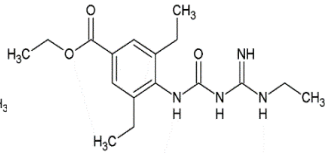
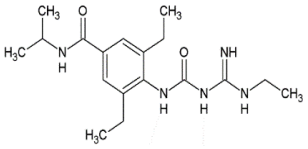
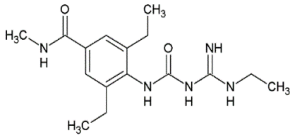
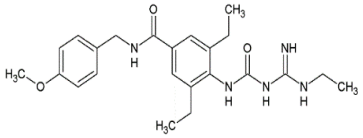
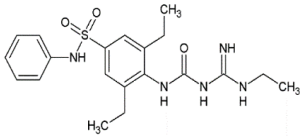
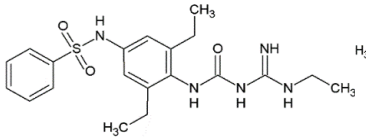
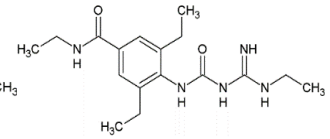
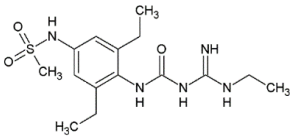
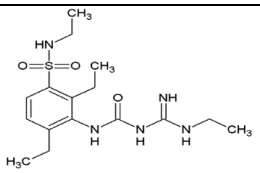
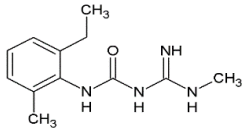
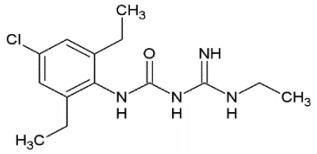
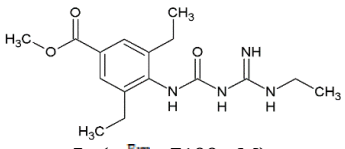
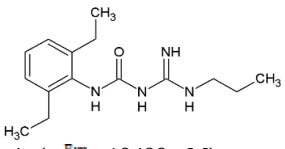
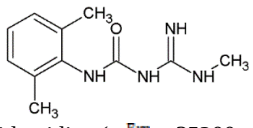
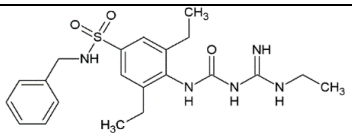
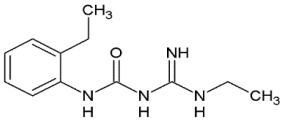
Furthermore, to mini mize systematic errors and highlight the impact of structural modifications, the relative binding free energy $\Delta\Delta G_{bind}$ (Eq. 3) was calculated for each derivative Li compared to the most active compound used as a reference L_{ref}:

$$\Delta\Delta G_{bind} = \Delta G_{bind}(Li) - \Delta G_{bind}\, L_{ref}$$

$$= \Delta\Delta E_{bind} + \Delta\Delta G_{solv} - T\Delta\Delta S_{conf} \quad \text{Eq. 3}$$

Univariate QSAR model development and statistical validation: The QSAR model was constructed and rigorously validated using QSARINS software version 2.2.4-2019, which specifically implements the validation protocols required by the OECD (Organization for Economic Cooperation and Development)[8-14].

Table 1: Structures and activities of ligands of the training set.

 5g (IC_{50}^{Exp}= 210 nM)	 5o (IC_{50}^{Exp} =700 nM)	 5c (IC_{50}^{Exp}= 2200 nM)
 5k (IC_{50}^{Exp}= 2500 nM)	 5f (IC_{50}^{Exp} = 2600 nM)	 5j (IC_{50}^{Exp} = 2800 nM)
 5h (IC_{50}^{Exp}= 3600 nM)	 5l (IC_{50}^{Exp} = 3600 nM)	 5r (IC_{50}^{Exp} = 3600 nM)
 5n (IC_{50}^{Exp} = 3800 nM)	 5i (IC_{50}^{Exp} = 4900 nM)	 5m (IC_{50}^{Exp} = 5200 nM)
 5q (IC_{50}^{Exp} = 6000 nM)	 4a (IC_{50}^{Exp} = 6200 nM)	 5a (IC_{50}^{Exp} = 6300 nM)
 5e (IC_{50}^{Exp}= 7100 nM)	 4c (IC_{50}^{Exp}= 10400 nM)	 Lidamidine (IC_{50}^{Exp} = 35200 nM)
 5s (IC_{50}^{Exp}= 36200 nM)	 4e (IC_{50}^{Exp}= 51400 nM)	

A univariate linear regression was established using the relative binding free energy $\Delta\Delta G_{bind}$ as the descriptor to predict the experimental biological activity IC_{50}^{Exp} as the response. The dataset (n=25) was split into a training set (n=20) and a validation set (n=5). To ensure the model's robustness, internal consistency, and external predictivity, the following statistical metrics were calculated:

- **Internal robustness**: Evaluated using the coefficient of determination R^2, Leave-One-Out cross-validation (LOOCV) R^2_{LOOCV}, and Leave-Many-Out cross-validation (LMOCV) R^2_{LMOCV}. We also compared the Root Mean Square Error (RMSE) and Mean Absolute Error (MAE) against their cross-validated counterparts ($RMSE_{CV}$) and (MAE_{CV}) to detect potential over-fitting.
- **External predictivity**: Assessed using the validation set through the squared correlation coefficient (R^2_{ext}), the Root Mean Square Error of

the validation set ($RMSE_{ext}$), and the Mean Absolute Error of the validation set (MAE_{ext}).

- **Y-Randomization test**: To confirm the correlation was not due to chance, 2000 iterations of Y-scrambling were performed. The resulting RYscr2 and the R_p^2 parameter (which adjusts the R^2 based on the randomization results) were used to confirm the model's statistical significance.
- **Applicability domain**: The structural and response reliability of the model was verified using the leverage approach. The warning leverage threshold (h*) was calculated using the formula h*=3p+1/n, where p is the number of descriptors and n is the number of training compounds. This statistical boundary was used to ensure that all predicted inhibitors fall within the defined chemical space of the training set and to identify any potential structural or response outliers.

Per-residue interaction energy decomposition

To identify the individual amino acids driving the molecular recognition process, per-residue interaction energy decomposition was performed. This analysis calculated the non-bonded interaction energy (Eint) between each active conformation of the ligands and the individual residues within the PptT binding pocket.

The total interaction energy for each residue (i) was determined by the sum of its van der Waals (E_{vdw}) and electrostatic (E_{elec}) components:

$$E_{int}(i) = E_{vdw}(i) + E_{elect}(i) \quad \text{Eq. 4}$$

This quantitative assessment allows for the identification of "hot-spot" residues that contribute most significantly to the complex stability. By pinpointing these critical residues, we can determine which specific molecular interactions such as hydrogen bonding, π-stacking, or hydrophobic contacts must be preserved or optimized in the design of next-generation amidinourea derivatives to enhance PptT affinity.

Molecular Dynamics Simulations (MDS)

The structural stability of the most active ligand and of new analogues, built from the native ligand, was evaluated by 200 ns molecular dynamics (MD) simulations, using the OPLS_2005 force field available in the Desmond module of Schrodinger 2018-4 software[15,16], as described recently[17].

MM-GBSA binding energy

After molecular dynamics, the average of the changes in binding free energy during complex formation was calculated over the all 200 nanoseconds and the last 50 nanoseconds of the trajectory using the molecular mechanics/generalized born surface (MM-GBSA) method[18]. The theory and method of MM-GBSA have been described in detail previously[19].

The change in binding free energy for each analogue $\Delta G_{MM\text{-}GBSA}$ was computed as:

$$\Delta G_{bind} = \Delta E_{MM} + \Delta G_{solv} + \Delta G_{SA} \quad \text{(Eq. 5)}$$

Where ΔE_{MM} represents molecular mechanics energy changes, ΔG_{solv} accounts for solvation effects, and ΔGSA represents surface area contributions.

Pharmacokinetic profile evaluation, and predictive description of the synthesis.

We employed machine learning to evaluate pharmacokinetic profiles. Tools such as pkCSM and mycoCSM, along with Schrödinger's QikProp program, were used to predict pharmacokinetic properties[20,21].

RESULTS

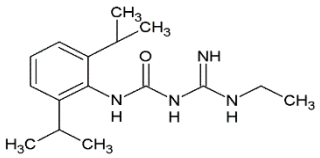
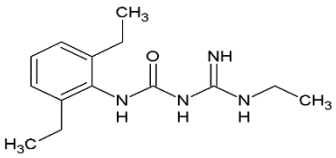
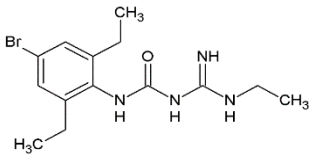
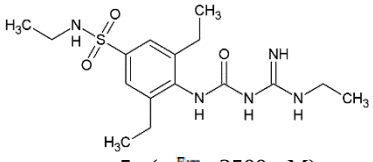
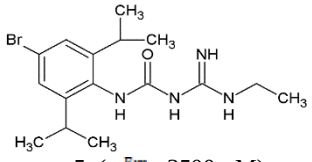
Dataset Partitioning

To ensure the robustness and external predictive power of the QSAR model, the 25 ligands were divided into training and validation subsets using a standard 80/20 ratio. This division was performed using the "Generate Training and Test Data" protocol within Discovery Studio®[6], where twenty (20) ligands (Table 1) were assigned to the training set to build the QSAR model, and five (05) ligands (Table 2) were reserved as an external validation set to independently verify its predictive accuracy.

Validation of the Molecular Docking Protocol

To confirm the reliability of the CDOCKER algorithm and the CHARMm force field in the context of the PptT binding pocket, a self-docking (redocking) study was performed. The co-crystallized ligand was extracted from the 6CT5 PDB structure and redocked into the active site using the parameters defined in the methodology.

Table 2: Structures and activities of the validation set.

		
4f (IC_{50}^{Exp}= 1200 nM)	AU8918 (IC_{50}^{Exp}= 2300 nM)	5b (IC_{50}^{Exp}= 2400 nM)
		
5p (IC_{50}^{Exp}= 3500 nM)	5t (IC_{50}^{Exp}= 3500 nM)	

The predicted binding pose demonstrated a good level of structural alignment with the experimental crystal orientation, yielding a Root Mean Square Deviation (RMSD) of 1.6 Å as shown in Figure 1. This value is well within the widely accepted 2.0 Å threshold for successful docking validation[15].

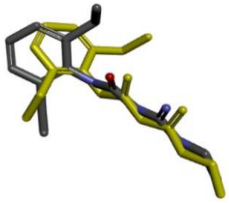


Figure 1: Structural alignment of cocristalized ligand (AU8918) and it's redocked pose.
(colored in yellow).

Molecular docking

The poses of ligands that have the same conformation after rigid docking as that of the endogenous ligand of the active site are selected (Figure 2). The different energies mentioned below are determined for these poses in complex with the enzyme.

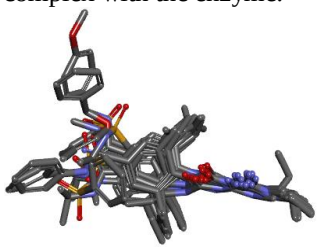


Figure 2: Superimposition of the best poses of 25 ligands.

Table 3: Relative binding free energies of complex formation between ligands from the training set and the enzyme, with $pIC_{50}^{Exp} = 9 - log_{10}(IC_{50}^{Exp})$.

Training set	$\Delta\Delta E_{bind} + \Delta\Delta G_{solv}$ [kcal.mol^{-1}]	$T\Delta\Delta S_{conf}$ [kcal.mol^{-1}]	$\Delta\Delta G_{bind}$ [kcal.mol^{-1}]	pIC_{50}^{Exp}
5g (ref)	0.00	0.00	0.0	6.68
5o	2.60	0.11	2.5	6.15
5c	6.44	-0.97	7.4	5.66
5k	5.60	-0.17	5.8	5.60
5f	5.70	-0.55	6.2	5.59
5j	5.16	-0.47	5.6	5.55
5h	4.66	-0.70	5.4	5.44
5l	6.39	0.27	6.1	5.44
5r	8.86	0.00	8.9	5.44
5n	10.03	-0.03	10.1	5.42
5i	7.14	-0.54	7.7	5.31
5m	9.13	-0.45	9.6	5.28
5q	9.85	-0.35	10.2	5.22
4a	9.32	-1.60	10.9	5.21
5a	9.01	-0.89	9.9	5.20
5e	10.06	-0.70	10.8	5.15
4c	8.69	-1.09	9.8	4.98
Lidamidine	11.09	-1.76	12.8	4.46
5s	12.43	-0.03	12.5	4.44
4e	13.78	-1.48	15.3	4.29

Table 4: Comparison of experimental and theoretical (obtained by $(Eq.6)$) pIC_{50} values from the validation set.

Validation set	$\Delta\Delta E_{bind} + \Delta\Delta G_{solv}$ [kcal.mol^{-1}]	$T\Delta\Delta S_{conf}$ [kcal.mol^{-1}]	$\Delta\Delta G_{bind}$ [kcal.mol^{-1}]	pIC_{50}^{Exp}	pIC_{50}^{Pred}	pIC_{50}^{Theo} / pIC_{50}^{Exp}
4f	4.43	-0.95	5.37	5.92	5.75	0.97
AU8918	6.19	-1.24	7.43	5.64	5.46	0.97
5b	6.73	-0.62	7.35	5.62	5.47	0.97
5p	10.42	-0.34	10.75	5.46	4.99	0.91
5t	8.76	-0.45	9.22	5.46	5.21	0.95

Statistical Quality and Robustness of the QSAR Model

The QSAR model (Eq. 5), developed using the relative binding free energy ($\Delta\Delta G_{bind}$) as the sole thermodynamic descriptor, demonstrated excellent statistical quality that complies with OECD rules. The resulting regression equation is:

$$pIC_{50}^{exp} = -0.1417*\Delta\Delta G_{bind} + 6.5117 \quad \text{Eq.6}$$

The model was constructed using a training set of 20 ligands. The experimental activities covered a broad biological range, with IC_{50}^{Exp} values spanning from 210 nM to 51,400 nM. We chose 5 g as a reference because it possesses greater biological activity. Furthermore, the activities are expressed in nanomolar (nM) units to facilitate better comparison, as our goal is to identify molecules with higher activity effectively shifting from the micromolar to the nanomolar range.

The ratio $pIC_{50}^{Theo} / pIC_{50}^{Exp} \cong 1$ shows that the model is good for estimating the activities of new molecules.

Internal robustness and fitting

The model showed a strong correlation with a coefficient of determination of 0.87 and a high Fisher F-test value of 125.79, indicating a highly significant linear relationship. Its internal stability was confirmed through rigorous cross-validation, yielding a Leave-

One-Out value (R^2_{LOOCV}) of 0.85 and a Leave-Many-Out (R^2_{LMOCV}) value of 0.84. Furthermore, there is a high degree of proximity between the error metrics specifically between the root-mean-square error RMSE of 0.19 and the root-mean-square error of cross-validation RMSECV of 0.21, as well as the corresponding mean absolute errors (MAE) of 0.17 and MAE_{CV} 0.18.

External predictivity

The predictive power of the model was successfully verified using an external validation set (n=5). The external squared correlation coefficient R^2_{ext} was 0.87, matching the training set's R^2.

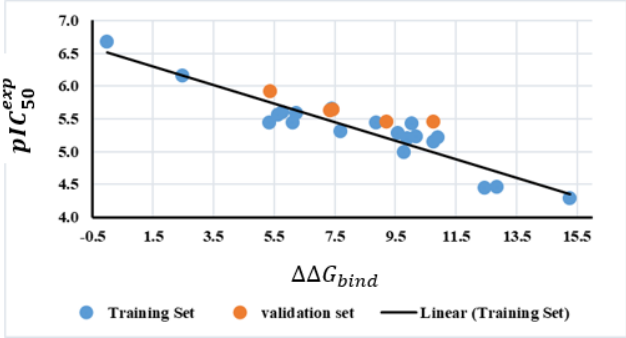


Figure 3:Correlation curve of pIC_{50}^{Exp}depending on $\Delta\Delta G_{Bind}$.

Table 5: QSAR model performance.

$pIC_{50}^{exp} = -0.1417 * \Delta\Delta G_{bind} + 6.5117$	
n	20
Range of activities (nM)	210 – 51400
Internal validation	
R^2	0.87
σ	0.2
Fischer F-Test	125.79
α	95%
Root mean square error $RMSE$	0.19
Mean absolute error MAE	0.17
R^2_{LOOCV}	0.85
R^2_{LMOCV}	0.84
$RMSE_{CV}$	0.21
MAE_{CV}	0.15
External validation	
R^2_{ext}	0.87
$RMSE_{ext}$	0.27
MAE_{ext}	0.25
Y-Randomization for 2000 iterations of shuffling	
R^2_{Yscr}	0.05
R^2_p	0.84

Y-Randomization (Y-scrambling)

To further validate the statistical significance of the model, a Y-randomization test (2000 iterations of shuffling) was performed. The resulting R^2_{yscr} was extremely low (0.05), while the R^2_p value of 0.84, being significantly higher than the recognized 0.5 threshold[12,16].

Applicability domain analysis

To ensure the reliability of the model's predictions, the structural applicability domain (AD) was evaluated using the leverage approach. The warning leverage threshold (h*) was calculated as 0.30, based on the training set size (n=20) and the single thermodynamic descriptor (p=1). A comprehensive analysis of the individual leverage values (h) revealed that all 25 amidinourea derivatives, including those in the external validation set, remained strictly below this threshold. Furthermore, no response outliers were identified, as all standardized residuals fell within the ±3 standard deviation limits.

Correlation Analysis of the QSAR Model

The relationship between the predicted thermodynamic descriptors and the experimental anti-tuberculosis activity is illustrated in Figure 3. The plot of experimental IC_{50}^{Exp} versus the calculated relative binding free energy $\Delta\Delta G_{bind}$ reveals a robust linear correlation for both the training set (blue circles) and the validation set (orange circles).

Per-residue interaction energy analysis

To gain a deeper understanding of the molecular basis of PptT inhibition, the total interaction energy was decomposed into individual residue contributions for the six representative compounds spanning the activity range (Table 6), from the most potent inhibitor 5g (IC_{50}^{exp} =210 nM) to the least active inhibitor 4e (IC_{50}^{exp}=51400 nM). This analysis identifies the "hot-

spot" residues that dictate the binding affinity and stability of the complexes.

Structural basis of differential biological activities

The variations in biological activity among the amidinourea derivatives can be directly attributed to the nature and strength of the interactions established within the PptT active site. The analysis of inhibitors 5g (IC_{50}^{Exp} =210 nM), 5n (IC_{50}^{Exp} =3800 nM), and 4e (IC_{50}^{Exp}=51400 nM) clearly demonstrates this.

The hydrophobic canal and stability

The presence of the hydrophobic canal, a critical feature identified in previous PptT studies[23,24], is clearly visualized through the extensive network of Van der Waals interactions in all complexes. Substituents in the para position on benzene, particularly aromatic ones, sometimes exhibit a stabilizing cation-π interaction with lysine 75, thus increasing ligand activity. Among these, although compound 5g is the most active, its ester function makes it relatively unstable during administration in humans, despite its superior *in vitro* affinity.

Key residue contributions to affinity

A comparative analysis of the quantitative energy contributions (Table 6) identifies the residues where enzyme-ligand affinity is maximized.

Table 6: Interaction energies (kcal/mol) of ligands with the active site of PptT.

	5g	5o	5n	5r	5s	4e
Phe153	-0.65	-0.84	-0.71	-0.61	-1.52	-0.75
Lys156	-2.71	-2.91	-1.92	-1.75	-2.34	-1.82
Glu157	-9.88	-10.64	-11.97	-11.98	-13.41	-10.91
Thr159	-0.64	-0.67	-0.40	-0.40	-0.54	-0.33
Tyr160	-5.67	-5.68	-6.07	-5.28	-5.51	-5.55
Lys161	-1.26	-0.44	-1.52	-0.62	0.61	-1.13
Trp170	-2.87	-2.62	-1.85	-2.80	-2.43	-1.91
Leu171	-3.58	-2.63	-1.62	-3.11	-2.48	-2.62
Gly172	-1.53	-1.50	-1.23	-1.47	-1.50	-1.32
Phe173	-6.11	-6.06	-4.48	-5.11	-5.47	-4.52
Asp175	-0.16	0.06	-0.09	-0.42	0.02	-0.19
Ala176	-0.55	-0.66	-0.83	-0.66	-0.64	-0.78
Ile178	-0.17	-0.15	-0.11	-0.13	-0.14	-0.09
COA301	-2.74	-7.21	-5.98	-3.43	-11.38	-5.00

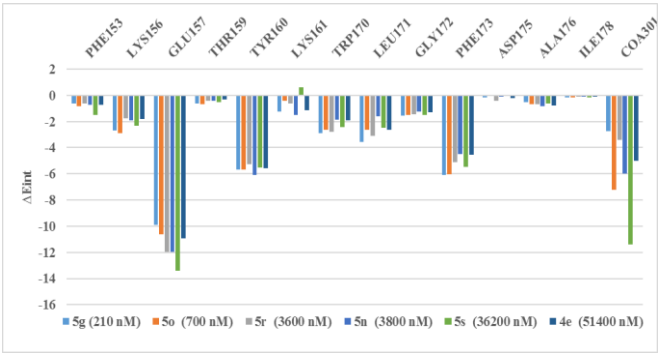


Figure 4:Interaction Energy contribution by residues.

Strategic implications for affinity improvement

The primary challenge in developing more potent anti-tuberculosis compounds lies in the ability to strategically maintain or intensify these specific structural interactions within the active site.

Docking and predicted activities of new analogues

To discover novel and more potent inhibitors against the *M. tuberculosis* PptT enzyme, an intuitive fragment substitution approach was conducted. Using the amidinourea core scaffold as a template, various chemical modifications were introduced across four positions (R^1, R^2, R^3, and R^4) utilizing a specialized structural library (Table 7). Docking of the new analogues is performed using the same parameters. Next, the free enthalpies of complex formation are calculated and their predicted inhibitory concentrations IC_{50}^{Pre} are deduced from the correlation equation of the model, (Eq.6: pIC_{50}^{exp} =-0.1417*$\Delta\Delta G_{bind}$+6.5117). The newly designed analogues were subjected to molecular docking simulations using the exact parameters validated in our previous protocol. Following pose generation, the binding free energies were computed, and their predicted median inhibitory concentrations IC_{50}^{Pre} were derived directly using the validated univariate correlation equation established in this work (Equation 6): pIC_{50}^{exp}= -0.1417*$\Delta\Delta G_{bind}$ + 6.5117. The calculated thermodynamic parameters, conformational entropy penalties $\Delta\Delta S_{conf}$, net binding free energies $\Delta\Delta G_{bind}$, and corresponding predicted biological activities for the top four design candidates are summarized in Table 8. Compound 5g is included as the high-potency reference standard from the experimental training set.

Interaction energies per residue of new amidinourea analogues

To uncover the physical forces driving this enhanced affinity, comparative per-residue interaction energy

decomposition ΔE_{int} was carried out for the designed analogues and the reference ligand 5g (Table 9).

Molecular dynamics

To evaluate the structural stability of the studied complexes, 200-ns molecular dynamics simulations were performed for the most active ligand from the training set (5g) and the top three analogues.

Pharmacokinetic profile evaluations

The pharmacokinetic descriptors for the best analogues as well as those for drugs currently used to treat *tuberculosis* or undergoing clinical trials are calculated using the QikProp and pkCSM programs.

MM-GBSA binding free energy

The mean MM-GBSA binding energy for the best compound in the training set (5g) and for the three best analogues AU_1-3-7-9, AU_1-7-6-11, and AU_1-6-2-10 was calculated over the last 50 nanoseconds of the trajectory (Table 10).

DISCUSSION

Validation of the Molecular Docking Protocol

The values confirm that the CDOCKER protocol effectively reproduced the native intermolecular interactions within the PptT binding pocket. Consequently, the validated protocol was deemed robust enough to explore the binding orientations and thermodynamic profiles of the 25 amidinourea derivatives.

Molecular docking, statistical quality and robustness of the QSAR model

We note that the model does not exhibit overfitting and possesses a high degree of internal consistency. Regarding external validation, the model's ability to accurately predict the antitubercular activity of new amidinourea derivatives is demonstrated. The Y-randomization test confirms that the correlation between the PptT binding free energy and anti-tuberculosis activity is not due to chance. The structural applicability domain (AD) using the leverage approach results confirm that all compounds reside within the model's domain of validity, ensuring that the predicted anti-tuberculosis activities are structurally and statistically good.

Per-residue interaction energy analysis

The energy profiles, illustrated in Figure 4, reveal that the binding stabilization is primarily localized within a specific cluster of residues and the co-crystallized COA301 cofactor.

- **Dominant electrostatic stabilization**: The Glu157 residue was found to be the amino acid that makes the most significant contribution. This suggests a powerful stabilizing effect, likely due to strong hydrogen bonding or electrostatic complementarity with the amidinourea scaffold.
- **Cofactor involvement**: Significant stabilizing contributions were observed with COA301, particularly for compound 5s. This indicates that the inhibitors establish a high-affinity interface not only with the PptT protein residues but also with the bound Coenzyme A molecule.
- **Key hydrophobic and polar contributors**: Tyr160, Gly172, and Trp170 also provided consistent stabilization across the series (-2 to -6 kcal/mol). The relative consistency of these values suggests they form the core structural framework of the binding pocket.
- **Potency Correlation**: Interestingly, while Glu157 provides the highest absolute energy, the variations in activity between 5g (210 nM) and the less active derivatives appear to be driven by subtle energy shifts across multiple residues, such as Phe153, Lys156, and Leu171.

Structural basis of differential biological activities

The analysis highlights three representative types of interactions: hydrogen bonds, van der Waals interactions, and electrostatic interactions. The strong electrostatic interaction between Glu157 and 5g is a primary driver of potency. As seen in the 2D maps (Figure 5), 5g establishes a salt bridge and pi-cation interaction, whereas less active molecules like 4e only maintain a single, weaker hydrogen bond.

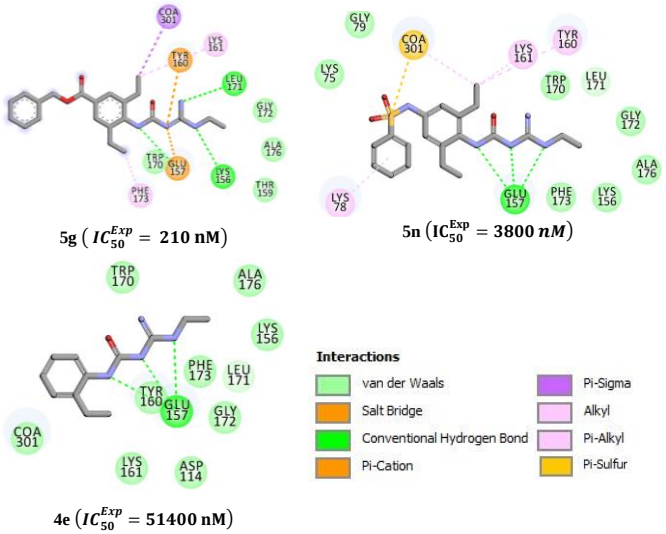


Figure 5: 2D diagrams of interactions between residues in the active site of PptT and: the most active ligand 5g; a moderately active ligand 5n and the least active ligand 4e.

Tyr160 and Phe173 form the structural framework of the pocket, providing the necessary hydrophobic anchoring for the aromatic scaffolds. Cofactor COA301 interactions also matter. Consistent with the energy decomposition, the most active molecules maintain high-affinity contact with the Coenzyme A cofactor, a relationship that diminishes significantly in the least active compound, 4e. The design process for the new analogues prioritized preserving the critical electrostatic network established with the Glu157, while simultaneously maximizing the van der Waals fit within the characteristic hydrophobic canal. Furthermore, maintaining the stabilizing interactions with key residues Tyr160 and Phe173, as well as the COA301 cofactor, is essential for preserving structural alignment. Finally, investigating targeted molecular modifications at the para position of the phenyl ring presents a promising pathway to introduce or intensify stabilizing interactions, which could simultaneously improve both target affinity and metabolic stability.

Table 7: Fragments R^1, R^2, R^3, and R^4 used in intuitive substitution to obtain new analogues of amidinourea derivatives.

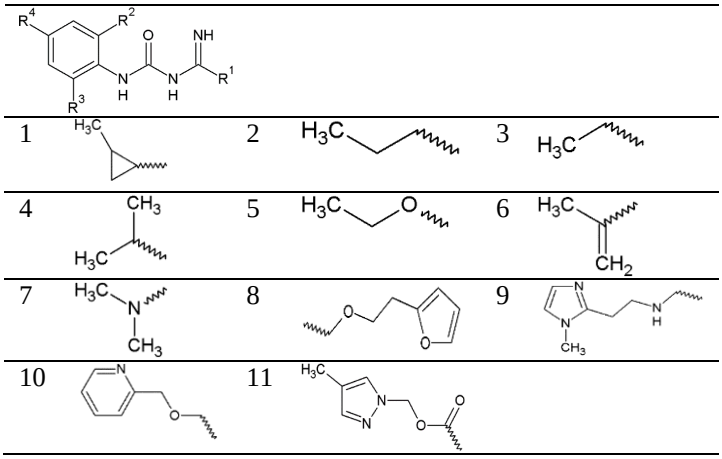


Table 8: Binding free energies (kcal.mol^{-1}) and predicted inhibition constant (nM) for the best of new analogues.

Analogues	$\Delta\Delta E_{Bind} + \Delta\Delta G_{solv}$	$T\Delta\Delta S_{conf}$	$\Delta\Delta G_{bind}$	pIC_{50}^{pre}	IC_{50}^{pre}
5g *(ref)*	0.00	0.00	0.00	6.68	210
AU_1-3-7-9	-8.80	0.15	-8.95	7.78	20
AU_1-7-6-11	-2.69	0.33	-5.12	7.24	60
AU_1-6-2-10	-0.12	0.27	-3.02	6.94	110

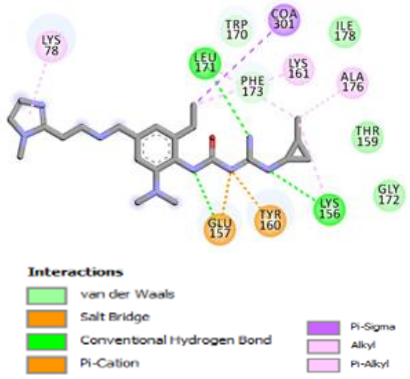


Figure 6: Interactions established by the best of the new analogue AU_1-3-7-9, ($IC_{50}^{pre} = 20\ nM$).

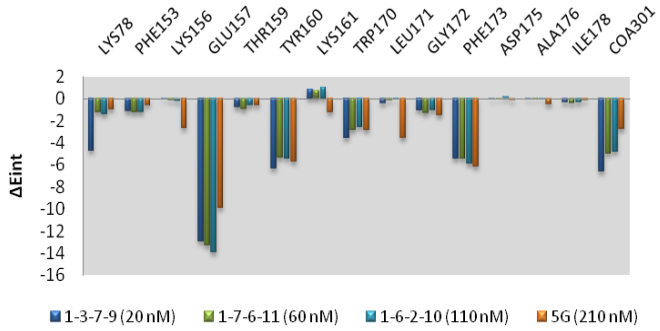


Figure 7: Interaction energies as individual contributions of the residues of the active site of PptT in complex with the best analogues and 5g (the most active ligand in the training set).

Table 9: Individual residue interaction energy contributions (kcal/mol) within the PptT active site.

	5g*	AU 1-3-7-9	AU 1-7-6-11	AU 1-6-2-10
Lys78	-1.01	-4.76	-1.24	-1.41
Phe153	-0.65	-1.15	-1.25	-1.23
Lys156	-2.71	0.05	-0.21	-0.23
Glu157	-9.88	-12.93	-13.28	-13.95
Thr159	-0.64	-0.80	-0.95	-0.63
Tyr160	-5.67	-6.32	-5.39	-5.40
Lys161	-1.26	0.84	0.72	1.01
Trp170	-2.87	-3.57	-2.86	-2.62
Leu171	-3.58	-0.42	-0.20	-0.11
Gly172	-1.53	-1.09	-1.32	-1.02
Phe173	-6.11	-5.40	-5.46	-5.90
Asp175	-0.16	-0.08	0.02	0.16
Ala176	-0.55	-0.07	-0.12	-0.08
Ile178	-0.17	-0.39	-0.40	-0.37
COA301	-2.74	-6.56	-4.97	-4.83

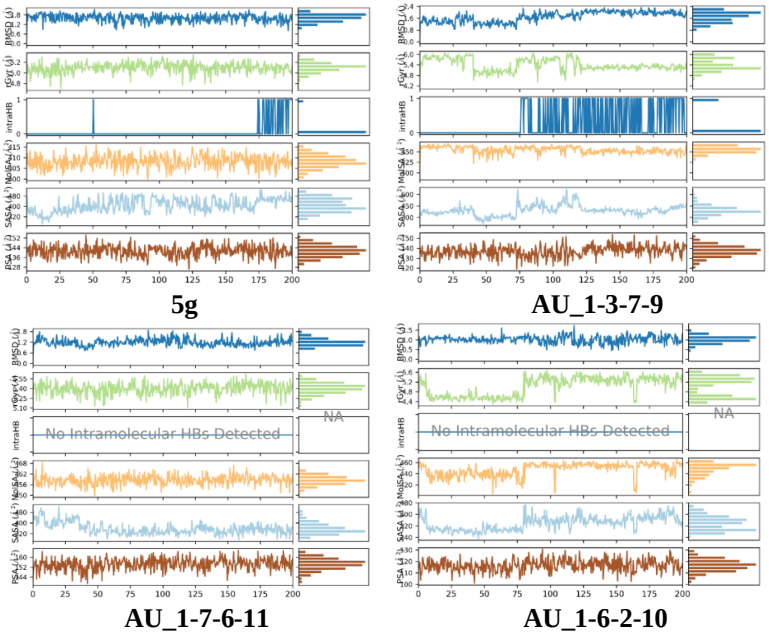


Figure 8: Time-evolution of the properties of the ligand-PptT complexes during 200 ns MD simulation.

For each inhibitor, top to bottom: plot of the root mean square deviation (RMSD) with respect to the initial conformation vs. The simulation time, radius of gyration (rGyr), number of intramolecular hydrogen bonds (intraHB), molecular surface area (molSA), solvent-accessible surface area (SASA), and polar surface area (PSA).

Docking and predicted activities of new analogues

The systematic substitutions at the R^1 to R^4 positions led to a distinct increase in target binding affinity compared to the parent training series. Most notably, analogue AU_1-3-7-9 (Figure 6) exhibited a remarkably favorable net free energy of binding ($\Delta\Delta G_{bind}$=-8.95 kcal.mol-1), translating to an outstanding predicted potency of IC_{50}^{Pre}=20 nM. This marks a 10-fold increase in anti-*tuberculosis* activity over the best experimental compound 5g IC_{50}^{exp}=210 nM.

Interaction Energies per Residue of New Amidinourea Analogues

The predicted biological activity of the best AU_1-3-7-9 analogue can be explained by a significant increase in hydrophobic interactions at positions R^1 and R^4 with the Lys78 residue. All of these interactions observed with the residues justify the activity of the new analogues. The new analogues interacts with several residues in the active site of PptT. These residues play an essential role in enhancing the inhibitory activity of the new amidinourea analogues. The diagram shows that the best analogue retains its affinity for Phe173 and has increased affinity for Glu157, Tyr160, Trp170, and COA301. Furthermore, this new analogue establishes a stabilizing interaction with Lys78. Consequently, interactions with the enzyme are more favorable for the best analog than for the 5g ligand.

Molecular dynamics

The temporal evolution of various properties of the bound inhibitors, such as root mean square deviation (RMSD) from the initial conformation, radius of gyration (rGyr), number of intramolecular hydrogen bonds (intraHB), molecular surface area (molSA), solvent-accessible surface area (SASA), and polar surface area (PSA), is satisfactory. Examination of the root-mean-square deviations (RMSD) highlights good structural convergence. The conformational equilibrium of the systems is not affected. The [system/complex] maintains the radius of gyration (rGyr) an invariant value at 5.1 Å, reflecting high rigidity and dynamic stability.

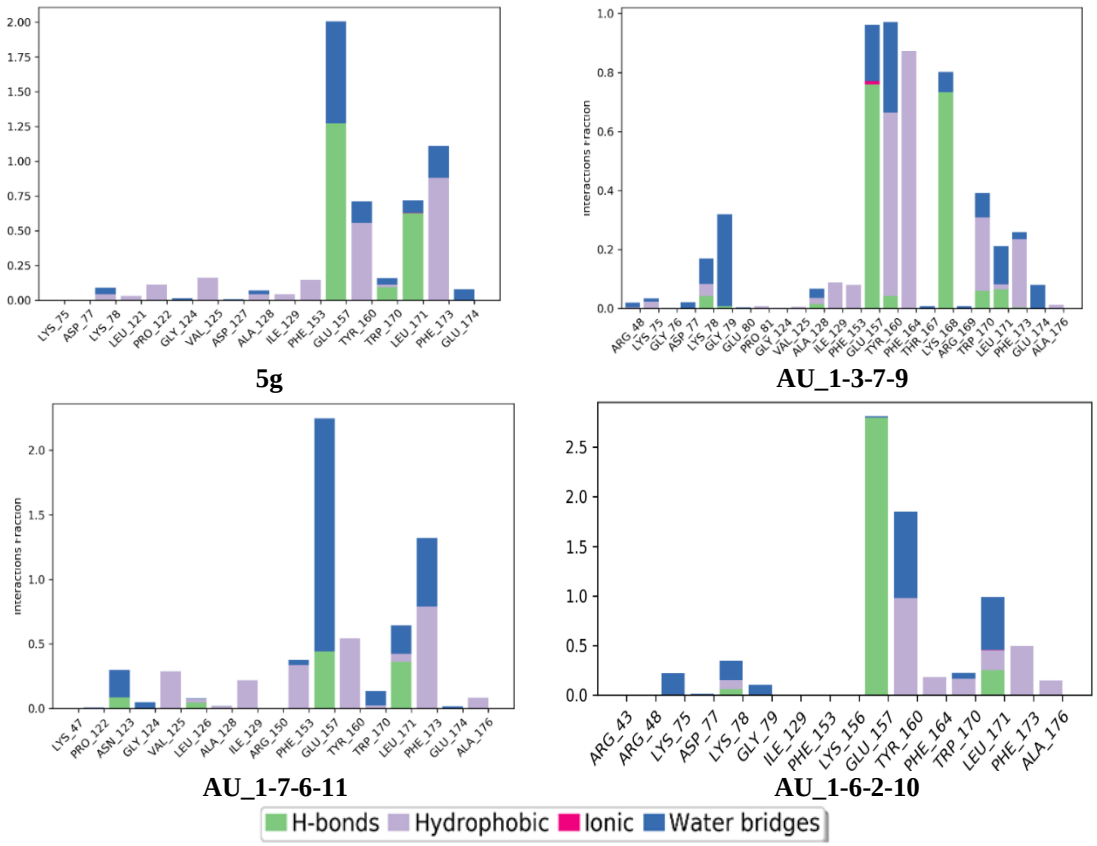
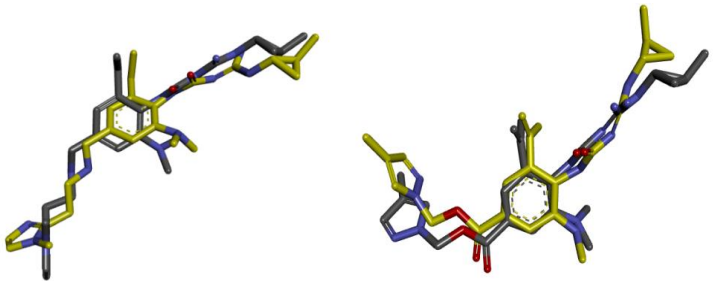


Figure 9: Contribution of individual active site residues to inhibitor binding in ligand-PptT complexes present during MD simulations: HB (green); ionic interactions (magenta); hydrophobic contacts (purple); water bridges (blue).

Table 10: Variation of the binding free energy ($\Delta\Delta G_{MM-GBSA}$) of the analogues.

Analogues	$\Delta\Delta G_{bind}$ [kcal.mol^{-1}]	$\Delta\Delta G_{MM-GBSA}$-last50ns [kcal.mol^{-1}]	IC_{50}^{pre} [^{n}M]
5g *(ref)*	0.0	0	210
AU_1-3-7-9	-8.9	-29.5	20
AU_1-7-6-11	-5.1	-14.6	60
AU_1-6-2-10	-3.0	-11.8	110



AU_1-3-7-9 (RMSD = 1.77 Å) **AU_1-7-6-11 (RMSD = 1.70 Å)**

Figure 10: Overlay of the ligand active conformations from complexes refined by molecular mechanics and averaged active conformations (yellow) resulting from MD simulations.

The display rGyr values of analogues confirm the preservation of a folded and compact conformation.

Pharmacokinetic profile evaluations

The values given by QikProp and pkCSM programs remain within the prescribed limits. For mycoCSM program, we have a high Maximum Recommended Tolerated Doses (MRTD) because it is greater than 0.477 log (mg/kg/day).

MM-GBSA Binding Free Energy

The negative values obtained during enzyme-ligand complex formation indicate that the interactions occur spontaneously. These values, which remain lower for the new analogues, compared to that of the 5g ligand, denote a higher affinity between the new inhibitors and the target protein. These values are also compared to the relative free energy of binding (PBSA). The biological activities fall within the same order of magnitude as each of these two thermodynamic quantities. This convergence confirms the reliability of the computational approaches and allows us to propose these designed analogues as potential inhibitors[25].

Table 11: ADME properties of the designed lead AU8918 analogues and known antitubercular drugs currently in clinical use or test, computed by QikProp (Schrödinger, 2018-4).

Compounds[a]	#stars[b]	M_W[c] [g/mol]	S_{mol}[d] [Å²]	$S_{mol,hfo}$[e] [Å²]	V_{mol}[f] [Å³]	RotB[g]	HB_{don}[h]	HB_{acc}[i]	logPo/w[j]	$logS_{wat}$[k]	$logK_{HSA}$[l]	logB/B[m]	BIP_{Caco}[n] [nm/s]	#metab[o]	IC_{50}^{pre} [nM]	HOA[q]	%HOA[r]
5g	1	396.5	744.2	392.0	1326.4	8	2	3	4.9	-6.6	0.9	-1.3	452.5	3	210*	1	100
AU_1-3-7-9	1	440.6	751.2	561.1	1432.9	10	3	5	4.1	-4.7	0.6	-0.6	292.6	6	20	3	95.3
AU_1-7-6-11	2	453.5	846.9	577.0	1505.4	9	2	7	4.7	-7.5	0.9	-1.8	347.9	5	60	1	100
AU_1-6-2-10	1	435.6	810.2	513.9	1473.0	11	2	5.2	5.8	-7.2	1.1	-1.1	1289.7	7	110	1	100
Bedaquiline	4	555.5	787	213.7	1532	9	1	3.8	7.6	-7	1.7	0.4	1562.2	5		1	100
Pretomanid	0	359.3	570.6	125.4	976	5	0	5.2	2.9	-4	-0.2	-0.7	612	2		3	94.1
Lignezolide	0	337.4	586.9	357.2	1026.6	2	1	8.7	0.5	-2	-0.7	-0.6	395.2	1		3	76.3
Clofazimine	4	473.4	816.4	113	1466.6	4	1	3	8.2	-10.1	1.9	0.3	5056.8	2		1	100
Sutezolid	1	353.4	605	339.3	1060.9	2	1	7.5	1.3	-3.4	-0.4	-0.5	401.7	0		3	81.4
Delamanid	3	534.5	865.6	272.6	1536.6	7	0	6	6.1	-8.9	1.2	-1.5	284.9	2		1	80.7
Pyrazinamide	3	123.1	300.4	0	444.4	1	2	5	-0.6	-0.5	-0.8	-0.7	307.7	4		2	67.8
Gatifloxacin	0	375.4	603.7	350.6	1105.5	2	1	6.75	0.6	-4.1	0.1	-0.6	17.8	1		2	52.7
Moxifloxacin	0	401.4	614.3	374.6	1159.2	2	1	6.75	1	-4.3	0.2	-0.4	24.8	1		2	58
Rifapentine	16	828.9	1145.5	699.6	2324.6	23	4	23.5	-2.1	2	-1.2	-4.6	0	12		1	0
Ofloxacin	0	361.4	600	348.7	1060.7	1	0	7.25	-0.4	-3.2	-0.4	-0.5	23.5	1		2	49.2
Amikacin	14	614.6	822.5	341	1622	22	19	28.1	-9.4	2	-2.2	-4.8	0	15		1	0
Kanamycin	17	786.7	1179.9	431.6	2186.1	26	12	28.8	-3.8	-2.9	-2.4	-8.6	0.1	13		1	0
Imipenem	0	299.3	487	259.1	880	8	3	7.2	1	-2	-0.7	-1.4	35	3		3	61
Amoxicilline	1	365.4	639.9	170.6	1101.7	6	4.25	8	-2.4	-2.1	-1.1	-2.4	0.4	5		1	6.7

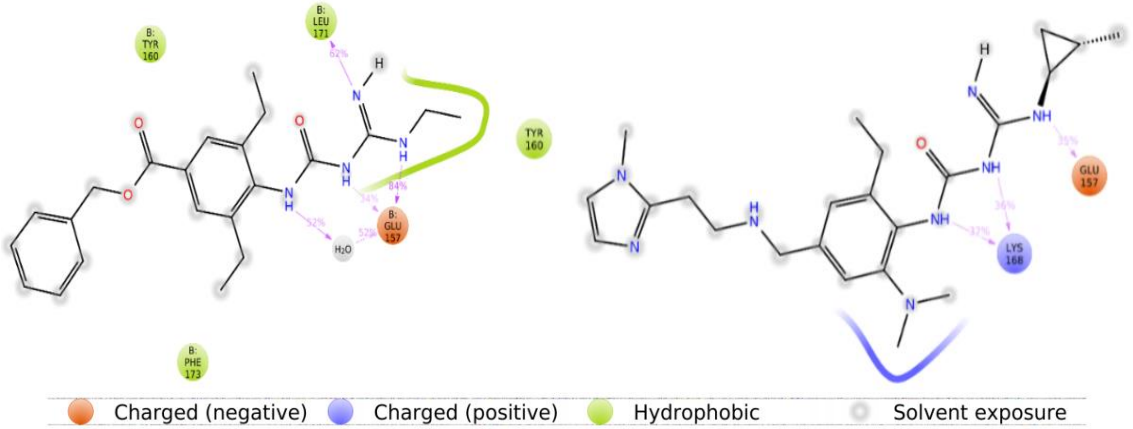


Figure 11: 2D representation of the most populated attractive interactions between the function groups of the 5g and best new inhibitor and the individual residues at the active site of PptT that occur in at least in 1/3 of the 500 analyzed frame.

Table 12: Predicting small-molecule pharmacokinetic and toxicity properties using graph-based signatures by (pkCSM).

Property	Model Name	Value				Unit
		AU_1-3-7-9	AU_ 1-7-6-11	AU _1-6-2-10	5g	
Molecule properties	Molecular Weight	440.6	453.5	435.6	396.5	[g/mol]
	LogP	2.43	3.159	4.84	3.83	
	Rotatable Bonds	9	7	9	7	
	Acceptors	6	7	4	4	
	Donors	5	4	4	4	
	Surface Area	190.04	193.04	189.73	170.91	
Absorption	Water solubility	-2.71	-2.93	-3.08	-3.07	Numeric (log mol/L)
	Caco2 permeability	0.41	0.489	0.35	0.70	Numeric (log Papp in 10-6 cm/s)
	Intestinal absorption	67.37	76.59	82.34	76.71	Numeric (% Absorbed)
	Skin Permeability	-2.73	-2.73	-2.73	-2.73	Numeric (log Kp)
	P-glycoprotein substrate	Yes	Yes	Yes	Yes	Categorical (Yes/No)
	P-glycoproteinI inhibitor	Yes	No	Yes	Yes	Categorical (Yes/No)
	P-glycoproteinII inhibitor	No	No	No	No	Categorical (Yes/No)
Distribution	VDss (human)	0.55	0.32	0.84	0.69	Numeric (log L/kg)
	Fraction unbound (human)	0.46	0.37	0.21	0.18	Numeric (Fu)
	BBB permeability	-1.21	-1.45	-1.28	-1.09	Numeric (log BB)
	CNS permeability	-3.43	-3.46	-2.44	-2.48	Numeric (log PS)
Metabolism	CYP2D6 substrate	No	No	No	No	Categorical (Yes/No)
	CYP3A4 substrate	No	No	No	No	Categorical (Yes/No)
	CYP1A2 inhibitor	No	No	No	No	Categorical (Yes/No)
	CYP2C19 inhibitor	No	No	No	No	Categorical (Yes/No)
	CYP2C9 inhibitor	No	No	Yes	No	Categorical (Yes/No)
	CYP2D6 inhibitor	No	No	No	No	Categorical (Yes/No)
	CYP3A4 inhibitor	No	No	Yes	No	Categorical (Yes/No)
Excretion	Total Clearance	0.98	0.67	1.17	0.75	Numeric (log ml/min/kg)
	RenalOCT2 substrate	Yes	No	No	Yes	Categorical (Yes/No)
Toxicity	AMES toxicity	Yes	No	No	No	Categorical (Yes/No)
	Max. Tolerated dose (human)	0.55	0.73	0.98	0.68	Numeric (log mg/kg/day)
	hERG I inhibitor	No	No	No	No	Categorical (Yes/No)

Table 13: Drug penetration predictions for all 8 organism-specific models, general Mycobacteria model and Maximum Recommended Tolerated Doses (MRTD) in human (mycoCSM).

Analogues Model	AU_1-3-7-9	AU_ 1-7-6-11	AU _1-6-2-10	5g
M. avium	-4.764	-4.329	-4.542	-4.393
M. bovis	-5.436	-5.517	-5.750	-5.410
M. fortuitum	-3.991	-4.023	-4.039	-4.231
M. intracellulare	-4.297	-4.409	-4.429	-4.662
M. kansasii	-4.671	-4.916	-4.401	-4.145
M. phlei	-4.529	-4.185	-4.674	-4.046
M. smegmatis	-4.463	-4.437	-4.337	-4.249
M. tuberculosis	-5.050	-4.595	-5.052	-4.656
General Mycobacteria	11.303	8.223	11.067	8.860
Caseum FU (%)	10.581	7.697	2.261	6.599
MRTD log (mg/kg/day)	0.549	0.727	0.982	0.685

Limitation of the study

We note here that intuitive substitution has limited the potential for generating a large number of analogues and, consequently, compounds with the prospect of improved activity. Furthermore, our computational resources do not allow for molecular dynamics simulations exceeding 200 ns.

CONCLUSIONS

This study utilized molecular docking, binding free energy decomposition, and Quantitative Structure-Activity Relationship (QSAR) workflows to characterize and strategically enhance a series of twenty-five (25) amidinourea derivatives targeting *M. tuberculosis* Phosphopantetheinyl Transferase (PptT). The constructed univariate model demonstrates impressive predictive strength, with its physics-based relative free energy of complex formation $\Delta\Delta G_{bind}$ accounting for 87% of the total variation in experimental biological activity. Deep analysis of the receptor-ligand complex networks shows that structural stability is primarily governed by strong hydrogen bonding networks and key non-polar contacts within the enzyme's conserved hydrophobic canal. By applying these insights to a targeted fragment library, we successfully engineered novel sub-series options. The top-designed candidate, analogue AU_1-3-7-9, displayed exceptional active-site comple-mentarity, highlighted by an advanced electrostatic salt-bridge network with Glu157, hydrophobic interactions with Lys75 and Phe164, localized interactions with Lys78, Lys168, and a powerful binding synergy with the embedded COA301 cofactor. These optimizations yielded a highly favorable thermodynamic state and a projected biological potency of 20 nM. This reflects a significant 10-fold improvement over the best experimental hit in the dataset. Other more robust methods involving, for example, Gibbs free enthalpy as a descriptor, combining a virtual chemical library screened by a pharmacophore model could make it possible to obtain PptT inhibitors with a higher power factor.

ACKNOWLEDGEMENTS

The authors gratefully acknowledge Prof. Paola Gramatica for granting a free license for the QSARINS software.

AUTHOR'S CONTRIBUTION

Kouakou KJL: conceptualization, writing original draft. **Kra KA:** conceptualization, investigations, computing, and editing. **Esmel EA:** conceptualization, investigations, technical, computational coaching, software, and editing. **Kéita M:** conceptualization, Intellectual input and final manuscript editing. **Megnassan E:** Intellectual input and final manuscript editing. Final manuscript was checked and approved by all authors.

DATA AVAILABILITY

Data will be available on request to anyone from the correspondence author.

CONFLICT OF INTERESTS

The authors declared no conflict of interests

REFERENCES

1. Rastogi N, Legrand E, Sola C. The mycobacteria: An introduction to nomenclature and pathogenesis. Rev Sci Tech 2001; 20: 21-54. *https://doi.org/10.20506/rst.20.1.1265*
2. Koloma I. Role of biological sex in the immune response against the *Mycobacterium tuberculosis* complex (Doctoral dissertation, USTTB). 2021
3. WHO. Tuberculosis Global Report 2025.
4. Germain MA, Latrille CFR, Philippon A, *et al*. Lymph: From Antiquity to the 21st Century. L'Harmattan Publishers; 2023.
5. Ottavi S, Scarry SM, Mosior J, *et al*. *In vitro* and *in vivo* inhibition of the mycobacterium tuberculosis phosphor pante theinyl transferase by amidinoureas. J Med Chem 2022; 65: 1996-2022. *https://doi.org/10.1021/acs.jmedchem.1c01565*
6. Biovia. Discovery Studio molecular modeling and simulation program n.d.
7. Ballinger E, Mosior J, Hartman T, *et al*. Opposing reactions in coenzyme A metabolism sensitize *Mycobacterium tuberculosis* to enzyme inhibition. Science (1979) 2019; 363: eaau8959. *https://doi.org/10.1126/science.aau8959*
8. Gramatica P, Cassani S, Roy PP, *et al*. QSAR modeling is not push a button and find a correlation: a case study of toxicity of (benzo-)triazoles on algae. Mol Inform 2012; 31: 817-35. *https://doi.org/https://doi.org/10.1002/minf.201200075*
9. Gramatica P, Chirico N, Papa E, *et al*. QSARINS: A new software for the development, analysis, and validation of QSAR MLR models. J Comput Chem 2013; 34: 2121-32. *https://doi.org/https://doi.org/10.1002/jcc.23361*
10. Gramatica P, Cassani S, Chirico N. QSARINS-chem: Insubria datasets and new QSAR/QSPR models for environmental

pollutants in QSARINS. J Comput Chem 2014; 35: 1036-44. *https://doi.org/https://doi.org/10.1002/jcc.23576*

11. Gramatica P, Sangion A. A historical excursus on the statistical validation parameters for QSAR models: A clarification concerning metrics and terminology. J Chem Inf Model 2016; 56: 1127-31. *https://doi.org/10.1021/acs.jcim.6b00088*
12. Gramatica P. Principles of QSAR Modeling: Comments and suggestions from personal experience. Int J Quantitative Structure-Property Relationships 2020; 5: 61-97. *https://doi.org/10.4018/IJQSPR.20200701.oa1*
13. Gramatica P. Origin of the OECD Principles for QSAR validation and their role in changing the QSAR paradigm worldwide: An Historical Overview. J Chemom 2025; 39: e70014. *https://doi.org/https://doi.org/10.1002/cem.70014.*
14. Chirico N, Sangion A, Gramatica P, *et al*. QSARINS-Chem standalone version: A new platform-independent software to profile chemicals for physicochemical properties, fate, and toxicity 2021; 42. John Wiley & Sons, Ltd. *https://doi.org/https://doi.org/10.1002/jcc.26551*
15. Schrödinger LLC, D. E. Shaw Research, Desmond Molecular Dynamics System 2018.
16. De Vivo M, Masetti M, Bottegoni G. Role of molecular dynamics and related methods in drug discovery. J Med Chem 2021; 59(9): 4035-4061. *https://doi.org/10.1021/acs.jmedchem.5b01684*
17. Frecer V, Miertus S. Antiviral agents against COVID-19: Structure-based design of specific peptidomimetic inhibitors of SARS-CoV-2 main protease. RSC Adv 10 (2020) 40244-40263. *https://doi.org/10.1039/D0RA08304F*
18. T Hou, J Wang, Y Li, *et al*. Assessing the performance of the MM/PBSA and MM/GBSA methods. The accuracy of binding free energy calculations based on molecular dynamics simulations. J Chem Inf Model 2011; 51: 69-82. *https://doi.org/10.1021/ci100275a*
19. Ntie-Kang F, Kannan S, Wichapong K, *et al*, Binding of pyrazole-based inhibitors to Mycobacterium tuberculosis pantothenatesynthetase: Docking and MM-GB(PB)SA analysis. Mol Biosyst 2014; 10: 223-239. *https://doi.org/10.1039/C3MB70449A*
20. Pires DE, Blundell TL, Ascher DB. PkCSM: Predicting small-molecule pharmacokinetic properties using graph-based signatures (Theory-How to EnterpretPkCSM Result) 2015. *https://doi.org/10.1021/acs.jmedchem.5b00104*
21. Pires DE, Ascher DB. MycoCSM: using graph-based signatures to identify safe potent hits against mycobacteria. J Chem Inform Model 2020; 60(7): 3450-3456. *https://doi.org/10.1021/acs.jcim.0c00362*
22. Leblanc C, Prudhomme T, Tabouret G, *et al*. 4′-Phosphopantetheinyl Transferase PptT, a new drug target required for *Mycobacterium tuberculosis* growth and persistence *in vivo*. PLoS Pathog 2012, 8, No. e1003097. *https://doi.org/10.1371/journal.ppat.1003097*
23. Vickery CR, Kosa NM, Casavant EP, *et al*. Structure, biochemistry, and inhibition of essential 4′-phosphopantetheinyl transferases from two species of mycobacteria. ACS Chem Biol 2014; 9: 1939−1944. *https://doi.org/10.1021/cb500263p*
24. Jung J, Bashiri G, Johnston JM, *et al*. Crystal structure of the essential *Mycobacterium tuberculosis* Phosphopantetheinyl Transferase PptT, solved as a fusion protein with maltose binding protein. J Struct Biol 2014; 188: 274−278. *https://doi.org/10.1016/j.jsb.2014.10.004*
25. Yavo BU, Esmel AE, Kouakou KJL, Kéita M, Eugène M. Molecular modeling and virtual screening for computer-aided design of HCV NS5B polymerase inhibitors. Universal J Pharm Res 2026; 11(3): 43-57. *http://doi.org/10.22270/ujpr.v11i3.1586*